Mirror symmetry breaking as a problem in dynamic critical phenomena

David Hochberg* and María Paz Zorzano†
Centro de Astrobiología (CSIC-INTA), Carretera Ajalvir Kilómetro 4, 28850 Torrejón de Ardoz, Madrid, Spain
(Received 1 March 2007; published 16 August 2007)

The critical properties of the Frank model of spontaneous chiral synthesis are discussed by applying results from the field theoretic renormalization group (RG). The long time and long wavelength features of this microscopic reaction scheme belong to the same universality class as multicolored directed percolation processes. Thus the following RG fixed points (FPs) govern the critical dynamics of the Frank model for $d<4$: one unstable FP that corresponds to complete decoupling between the two enantiomers, a saddle point that corresponds to symmetric interspecies coupling, and two stable FPs that individually correspond to unidirectional couplings between the two chiral molecules. These latter two FPs are associated with the breakdown of mirror or chiral symmetry. In this simplified model of molecular synthesis, homochirality is a natural consequence of the intrinsic reaction noise in the critical regime, which corresponds to extremely dilute chemical systems.

DOI: 10.1103/PhysRevE.76.021109 PACS number(s): 05.70.Jk, 64.60.Ak, 05.10.Gg

I. INTRODUCTION

Mirror symmetry is broken in the bio-organic world and life as we know it is invariably linked to biological homochirality. An outstanding problem associated with the origin of life is to explain chiral symmetry breaking in nature, why for example, it came to be that the nucleotide links of RNA and DNA incorporate exclusively right-handed sugars while the enzymes involve only the left-handed amino acids. A recent survey of hypotheses concerning this phenomenon, experimental realizations, and additional pertinent bibliography can be found in Refs. [1–5].

The essential key ingredients of theoretical models of mirror-symmetry breaking processes in chemistry [4] include reactions in which the products serve as catalysts to produce more of themselves while inhibiting the production of their chiral or mirror-image counterparts. In chemistry, *enantiomers* are molecules that are nonsuperimposable complete mirror images of each other. Frank's original model [6], and a variant of which we study in this paper, involves autocatalysis of the two enantiomers, denoted here as L and D [7], and mutual inhibition or antagonistic effects between the two chiral species. More recently, Sandars introduced a model in which the detailed polymerization process and enantiomeric cross inhibition are taken into account, its basic features are explored numerically, but without including spatial extent, chiral bias, or noise [8]. Brandenburg and co-workers have analyzed further properties of Sandars' model and have proposed a truncated version including chiral bias [9], and have studied this reduction with spatial extent and coupling to a turbulent advection velocity [10]. Gleiser and Thorarinson analyze the reduced Sandars' model with spatial extent and coupling to an external white noise [11] and in [12], Gleiser considers the reduced chiral biased model with external noise. Despite the simplicity of the Frank model, ignoring as it does the polymerization process, it continues to serve as a kind of "Ising model" for chiral symmetry breaking, and the purpose of this paper is to better understand its critical properties by exploiting the model's relation to directed percolation phenomenology.

The specific reaction scheme we will study in this paper is given as follows. The k_i denote the reaction rate constants and we take the achiral substance A as a uniform constant background: Autocatalytic production:

$$L + A \underset{k_3}{\overset{k_1}{\rightleftharpoons}} L + L, \quad D + A \underset{k_3}{\overset{k_1}{\rightleftharpoons}} D + D. \tag{1}$$

Dimerization and additional mutual inhibition in second order reactions:

$$L + D \xrightarrow{k_2} P, \quad L + D \xrightarrow{k_4} L + A, \quad L + D \xrightarrow{k_5} D + A. \tag{2}$$

Spontaneous decay or recycling back to the achiral substrate:

$$L \xrightarrow{k_6} A, \quad D \xrightarrow{k_6} A. \tag{3}$$

The above scheme differs from the original Frank model [6] in the open-flow reactor nature of the process and the fact that the reaction Eq. (1) is allowed to be reversible ($k_3 \geq 0$). We assume that each enantiomer diffuses with the same diffusion constant D_0 and incorporate this feature into the master equation description of this process. We also account for two inhibitory or mutually antagonistic reactions, with associated rates k_4 and k_5, in addition to Frank's dimerization step, k_2. This scheme is a partial hybrid between the Frank model and the Avetisov and Goldanskii (AG) reaction [see, e.g., Eq. (13) of [1]]. Whereas Frank's original model gives rise to pure homoquiral states in which only one enantiomer is present, the complete AG model leads to chiral symmetric broken final states where both enantiomers are present in unequal proportions. Mirror symmetry is broken in the AG model, but the breaking is not absolute.

Both the above and Frank's 1953 scheme yield the same field-theoretic structure for the *effective action*, and more importantly, therefore belong to the same *universality class*. In our analysis, we allow for $k_4 \neq k_5$, as this leads to a rich fixed

*hochbergd@inta.es; http://www.cab.inta.es
†zorzanomm@inta.es

point structure in the critical regime of the model. This choice implicitly accounts for the influence of an external chiral field or bias. Of course, a chiral symmetric action and Langevin equations result from the "natural choice" $k_4=k_5$. The properties of the chirally unbiased model can be studied as a special case of the above scheme.

Chiral or mirror symmetry breaking is an example of a nonequilibrium phase transition which is attained when the control variable $(k_1A-k_6)\approx 0$ becomes small. A continuous, second order, transition is then induced from a fully active state, characterized by the simultaneous presence of both competing enantiomers accompanied by fluctuations in each chirality, to an inactive or absorbing state, in which only one enantiomer survives. This control parameter can be made small (or large) by simply adjusting the concentration of the achiral molecule A. This limit implies that the net amount of total chiral matter is vanishingly small, i.e., the chemical system is extremely dilute at criticality. This is because the autocatalytic amplification of the enantiomers is delicately balanced by their spontaneous decay. The purpose of this paper is to understand this specific critical behavior and the emergent properties of the Frank model as exposed quantitatively by applying results [13] from the field-theoretic renormalization group (RG). We describe a significant result in the field of molecular chirality, namely, symmetry breaking induced by internal reaction noise in extremely diluted systems with absolute enantioselective catalysis. Such a mechanism is vitally important for current scenarios of prebiotic chemistry, where it is commonly accepted that sufficiently high concentrations of organic compounds could not have been reached during the chemical evolution of the early earth.

We are interested in the long time and long wavelength properties as governed by the nature of the RG fixed points and the topology of the RG flow in the space of effective reaction rates. The statistical field theory derived from the scheme Eqs. (1)–(3) maps identically to an action for so-called multispecies directed percolation (MDP) [13], for the special case of two "colors" or species. Thanks to this correspondence, the full details of the RG analysis already carried out for MDP can be carried over and applied to analyze the critical chemical properties of the Frank model. In the next section, we present the field-theory action associated with the above scheme, which after a suitable rescaling, leads to the effective action that holds in the critical regime. In Sec. III we reproduce the complete RG flow diagram for this model. However, only a part of this flow diagram is applicable to real chemical systems, and we discuss the consequences for chiral symmetry breaking near criticality. In Sec. IV we derive the Langevin equations that individually hold in the vicinity of the saddle point and the two stable fixed points of that flow diagram and integrate these numerically to obtain the time dependence of the competing enantiomers for both large and small noise amplitudes. The results are briefly summarized in Sec. V where the significance of criticality for scenarios of prebiotic chemistry is emphasized. The relation between criticality and extremely diluted chemical systems is brought out in Appendix A. The modifications that must be made to the effective action when the dimerization and antagonistic reactions are allowed to be reversible are briefly discussed in Appendix B.

II. THE EFFECTIVE FIELD THEORY ACTION

The correct inclusion of the effects of microscopic density fluctuations in reaction-diffusion systems can be carried out once the kinetic scheme is specified. With the scheme in hand, we derive the corresponding chemical master equation, represent this process by creation and annihilation operators on a spatial lattice [14], and in the final step, upon taking the continuum limit, we pass to a path integral representation [15,16]. From this, an effective action S_{eff} can be straightforwardly derived which contains all the critical dynamics implied by the reaction scheme to be studied. The mapping of related kinetic schemes to continuum statistical path integrals is spelled out in [17,18] where the main steps can be found. Applying this procedure to the scheme in Eqs. (1)–(3) yields the complete action S governing the reaction dynamics:

$$S=\int d^d\mathbf{x}\int dt[a^*(\partial_t a-D_0\nabla^2 a+k_2ab-k_1Aa+k_6a+k_3a^2)+a^{*2}(k_3a^2-k_1Aa)+b^*(\partial_t b-D_0\nabla^2 b+k_2ab-k_1Ab+k_6b+k_3b^2)+b^{*2}(k_3b^2-k_1Ab)+k_2a^*b^*ab+k_4b^*ab+k_4a^*b^*ab+k_5a^*ab+k_5a^*b^*ab], \tag{4}$$

where d is the spatial dimension, and $a(\mathbf{x},t)$, $a^*(\mathbf{x},t)$, $b(\mathbf{x},t)$, and $b^*(\mathbf{x},t)$ are continuous fields. In the absence of noise (the mean field approximation) the fields $a(\mathbf{x},t),b(\mathbf{x},t)$ correspond to the coarse-grained local densities of the L and D enantiomers, respectively. With the noise properly restored, these fields are generally *complex*—as is the noise—and do not directly represent the physical densities. However, the spatial averages $\langle a(\mathbf{x},t)\rangle,\langle b(\mathbf{x},t)\rangle$ are indeed real and do correspond to the particle densities [19]. The quantities $a^*(\mathbf{x},t),b^*(\mathbf{x},t)$ represent the conjugate or response fields. These are intimately related to the fluctuations inherent in the system. In fact, when the action S depends quadratically on the conjugate fields, these can be integrated out exactly from the path integral, and the noise statistics completely and rigorously characterized [19]. The *noncritical* spatial dynamics [i.e., for $(k_1A-k_6)\gg 0$] implied by the action Eq. (4) with its attendant complex noise and fields was explored numerically in [18] for $k_4=k_5=0$ and $k_6=0$.

The fields are next rescaled in the action Eq. (4), for the purpose of determining which couplings (i.e., which combinations of the rate constants k_i) are going to be *irrelevant* in the strict sense of the RG. This step is needed in order to correctly identify the complete set of vertices that are required to construct a field-theoretic perturbation expansion of this action [16]. We make use of the observation that when $k_2=0$ and $k_4=k_5=0$, the action Eq. (4) reduces to that for two identical uncoupled copies of the single particle Gribov process. We therefore rescale the fields according to $a^*=\theta\psi^*$, $a=\theta^{-1}\psi$, $b^*=\theta\phi^*$, and $b=\theta^{-1}\phi$, where $\theta=\left(\frac{k_3}{k_1A}\right)^{1/2}$. The space and time dependent densities of L and D are given by ψ and ϕ, respectively. We define the new coupling $u_0=(k_1Ak_3)^{1/2}$. Introducing a length scale κ^{-1} and measuring time in units of κ^{-2} (i.e., $[D_0]=\kappa^0$), we find that the new fields have scaling dimension $\kappa^{d/2}$, while $[r]=[(k_6-k_1A)/D_0]=\kappa^2$ is a relevant perturbation in the RG sense. On the other hand, $[u_0]$

$=\kappa^{2-d/2}$, so this nonlinearity becomes marginal in $d_c=4$ dimensions. Thus we learn that $d=4$ is the *upper critical dimension* of the Frank model, below which the mean field approximation is incorrect. Note that $[k_2]=[k_3]=[k_4]=[k_5]=\kappa^{2-d}$, and hence these couplings are irrelevant compared to $[u_0]$: indeed, since, e.g., $[k_2/u_0]=\kappa^{-d/2}$, these particular rate constants may be omitted from the *effective* action. Doing so leads to the effective action, which takes the form

$$S_{eff}=\int d^d\mathbf{x}\int dt\{\psi^*[\partial_t+D_0(r-\nabla^2)]\psi-u_0(\psi^{*2}\psi-\psi^*\psi^2)+\phi^*[\partial_t+D_0(r-\nabla^2)]\phi-u_0(\phi^{*2}\phi-\phi^*\phi^2)+(k_2+k_4)\theta^{-1}\phi^*\psi\phi+(k_2+k_5)\theta^{-1}\psi^*\psi\phi\}. \quad (5)$$

Note that the decoupling of the two enantiomers occurs when $k_2=k_4=k_5=0$, in other words, for vanishing mutual inhibition and dimerization. In particular, we see that both the original Frank model and the extension treated in this paper do indeed lead to the *same* field-dependent structure for the effective action, Eq. (5).

III. CRITICAL BEHAVIOR

The field theoretic renormalization group (RG) can be applied to S_{eff} in order to study the nonequilibrium critical dynamics of this reaction-diffusion system (for a pedagogical review of this methodology, see [16]). The main purpose for employing RG techniques is that they lead to differential equations describing how the model parameters, in this case, the kinetic constants, transform under a change of length scale. As we are here interested in the infrared, or long wavelength, properties of the Frank model, we therefore consider the RG flow of the parameters in the long wavelength limit. In general, certain combinations of the kinetic constants will flow to various fixed point (FP) values that depend on the space dimension. Thus the flow diagram can be constructed revealing the critical properties of the underlying kinetic scheme. As it turns out, S_{eff} maps exactly to a field theory of so-called multispecies directed percolation (MDP), for the special case of two "colors" or species [13]. A complete and exhaustive RG analysis has already been carried out for the general model in [13], and as pointed out there, the required renormalization factors for MDP are provided by the single species Gribov or directed percolation process. As an immediate consequence, the parameter combination $(k_1Ak_3)^{1/2}/D_0=u_0/D_0$ flows under renormalization to the stable fixed point $u^*=\frac{1}{2}\sqrt{2\epsilon/3}$, where $\epsilon=4-d>0$.

We next turn to the two interspecies couplings, which from Eq. (5) are each seen to be proportional to the sum of the rates $u_{12}\propto(k_2+k_5)$ and $u_{21}\propto(k_2+k_4)$, respectively. The competition between the two enantiomers comes in through the dependence on the rate of dimerization k_2, as well as through k_4 and k_5. The complete RG analysis in [13] as applied to our model proves that, except for the point **D**, the interspecies parameters in S_{eff} will flow to one of the following d-dependent fixed point values:

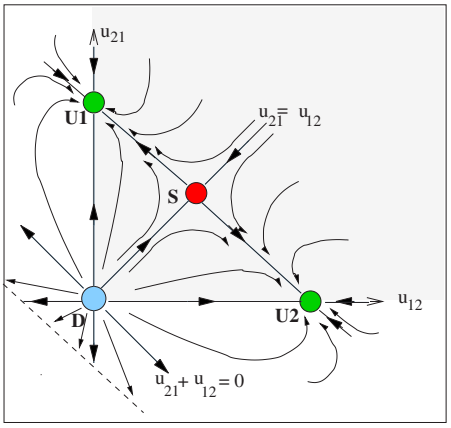

FIG. 1. (Color online) RG flow or "phase diagram" of the reaction scheme. Space of scale dependent renormalized couplings u_{12} and u_{21}. The shaded quadrant corresponds to the critical properties of the model with positive kinetic constants and diffusion. There is an unstable fixed point **D** at $(u_{12},u_{21})=(0,0)$ (blue dot); a saddle point **S** at $(u_{12},u_{21})=(u^*,u^*)$ (red dot), and two stable fixed points **U1** and **U2**, located at $(u_{12},u_{21})=(0,2u^*)$ and $(u_{12},u_{21})=(2u^*,0)$, respectively (green dots). The separatrix $u_{21}=u_{12}$ is the boundary between the basins of attraction of **U1** and **U2**. Outside this quadrant, the line $u_{21}+u_{12}=0$ separates the complete basin of attraction of **U1** and **U2** from the dashed line of fixed points $u_{12}+u_{21}=-2u^*$. See text and Ref. [13] for further details.

$$(u_{12},u_{21})\equiv\left(\frac{(k_2+k_5)\theta^{-1}}{D_0},\frac{(k_2+k_4)\theta^{-1}}{D_0}\right)\rightarrow\begin{cases}\mathbf{D}:(0,0), & \mathbf{S}:(u^*,u^*)\\ \mathbf{U1}:(0,2u^*), & \mathbf{U2}:(2u^*,0).\end{cases} \quad (6)$$

The point **D** corresponds to complete decoupling between the two enantiomers, **S** to a chiral symmetric coupling, whereas **U1** and **U2** each correspond to homochiral final states. The flow of the interspecies couplings u_{12} and u_{21} under renormalization is depicted in the flow diagram in Fig. 1. The flow, as indicated there by the sense of the arrows, corresponds to the critical large wavelength and long time properties of the microscopic model defined in Eqs. (1)–(3), and is reached for small values of $r\approx 0$. Thus the system goes critical when the difference in the rates of autocatalytic amplification (k_1A) and spontaneous decay (k_6) goes to zero. This is achieved by varying the concentration of the achiral matter A. This corresponds exactly to a situation of *extremely dilute* net chiral material characterized by $\psi+\phi\approx 0$ (see Appendix A for a simple proof of this fact). Note the topology of the flow and the stability property of each of the fixed points (**D**,**S**,**U1**,**U2**): (totally unstable, saddle point, stable, and stable), respectively.

We first consider the flow properties as depicted within the positive shaded quadrant $u_{12}>0$ and $u_{21}>0$ in Fig. 1. Insofar as it is reasonable to assume that the kinetic constants k_i and the diffusion D_0 are non-negative parameters, this is the most pertinent part of the full flow diagram for real chemical systems [20]. There is a totally unstable fixed point **D** located at the origin $u_{12}^*=u_{21}^*=0$. This corresponds to complete decoupling of the two enantiomers. But the only way to

arrive at this decoupled state is by blithely setting the initial values of $k_2=0$ as well as $k_4=k_5=0$ all to zero. Otherwise, the slightest positive deviation of any one of these rates from zero, drives the system eventually to either the saddle point **S**, if $\delta u_{12}=\delta u_{21}>0$, or to one of the two stable fixed points **U1**, if $\delta u_{21}>\delta u_{12}>0$ or **U2**, otherwise.

The diagonal symmetry line $u_{21}=u_{12}$ in this quadrant is a separatrix dividing the basins of attraction of the two unidirectional fixed points. For chirally symmetric kinetics, the natural choice of course is $k_4=k_5$, which puts the system dynamics directly on top of this separatrix. Then, as the diagram indicates, any positive initial value for $u_{21}=u_{12}>0$ drives the system to the chiral symmetric fixed point **S**. In this case, the final state of the system is determined by the fully symmetric couplings between the two enantiomers [see Eq. (6)]. In chemistry, a *racemic* mixture is one that contains equal amounts of left- and right-handed enantiomers of a chiral molecule. When the system is near the point **S**, racemic initial conditions lead to a racemic final state, while nonracemic initial conditions lead to a final state that maintains the original enantiomeric excess only for low noise amplitudes (see the numerical results in Sec. IV).

On the other hand, if the model has $k_4-k_5\neq 0$ which from Eq. (6) implies that $u_{21}\neq u_{12}$, then the system evolves to one of the two stable fixed points **U1** or **U2**. At either **U1** or **U2**, the system attains unidirectional interspecies couplings, see Eq. (6), which lead to the absolute amplification of one enantiomer at the expense of the other: that is, complete chiral symmetry breaking and a pure homochiral stable final state is the inevitable outcome (see the numerical results in Sec. IV).

For the sake of completeness, we now address the remainder of the flow diagram (the unshaded regions). In this case, there is then another separatrix whose equation is $u_{12}+u_{21}=0$, which divides the complete basin of attraction of the two unidirectional fixed points from the dashed line $u_{12}+u_{21}=-2u^*$; see Fig. 1. The parameter domain to the left of this dashed line corresponds to a region of instability, and it is conjectured in [13] that couplings satisfying the condition $u_{12}+u_{21}<0$ will lead to first order transitions. We hasten to point out, however, that this part of the diagram is only accessible if initial values of the u_{12} and or u_{21} are negative, corresponding to a *negative* diffusion $D_0<0$, provided, of course, that none of the reaction rates k_i are allowed to become negative [20]. Thus the region of this diagram applicable to real chemical systems is represented by the shaded quadrant.

IV. CRITICAL DYNAMICS

The temporal evolution of the two enantiomers in the critical regime represented in Fig. 1 is governed by a pair of coupled Langevin equations which follow straightforwardly from the effective action S_{eff}. These are obtained by carrying out a Gaussian integration over the conjugate fields ψ^* and ϕ^* in the path integral of the exponentiated effective action: $\int \mathcal{D}\psi \mathcal{D}\psi^* \mathcal{D}\phi \mathcal{D}\phi^* e^{-S_{eff}[\psi,\psi^*,\phi,\phi^*]}$. This final step yields a product of delta functional constraints under the integral which, in turn, lead to a pair of *exact* coupled stochastic partial differential equations [19]. The advantage of obtaining the Langevin equations in this way is that the noise properties are fully determined and do not have to be guessed at or put in by hand. Numerical solutions of these stochastic equations can be carried out to reveal the nature and qualitative tendency of the spatial and temporal evolution of the competing enantiomers in the neighborhood of each RG fixed point, as well as within their respective basins of attraction.

The Langevin equations that follow from S_{eff} are given by

$$\frac{\partial}{\partial t}\psi = D_0\nabla^2\psi + (k_1A - k_6)\psi - u_0\psi^2 - (k_2+k_5)\theta^{-1}\psi\phi + \xi_1, \tag{7}$$

$$\frac{\partial}{\partial t}\phi = D_0\nabla^2\phi + (k_1A - k_6)\phi - u_0\phi^2 - (k_2+k_4)\theta^{-1}\phi\psi + \xi_2, \tag{8}$$

where the noise satisfies $\langle\xi_1\rangle=\langle\xi_2\rangle=0$ and

$$\langle\xi_1(\mathbf{x},t)\xi_1(\mathbf{x}',t')\rangle = 2u_0\psi(\mathbf{x},t)\delta^d(\mathbf{x}-\mathbf{x}')\delta(t-t'), \tag{9}$$

$$\langle\xi_2(\mathbf{x},t)\xi_2(\mathbf{x}',t')\rangle = 2u_0\phi(\mathbf{x},t)\delta^d(\mathbf{x}-\mathbf{x}')\delta(t-t'). \tag{10}$$

These equations hold in the critical region shown in Fig. 1.

A. Langevin equations in the vicinity of the saddle point

In particular, the behavior of the model in the vicinity of the saddle point **S** where the interspecies couplings u_{12} and u_{21} flow to a symmetric fixed value, is given by the solutions of the system Eqs. (7), (8) where we now set $k_4=k_5$. These are subject to the noise Eqs. (9), (10), and we use the result that u_0/D_0 flows to u^*, together with the corresponding fixed point values for u_{12} and u_{21}, as given in Eq. (6). At this juncture, it is also convenient to rescale the fields $\tilde{\psi}=D_0u^*/(k_1A-k_6)\psi$, $\tilde{\phi}=D_0u^*/(k_1A-k_6)\phi$, and employ dimensionless time $\tau=(k_1A-k_6)t$ and coordinates $\hat{x}_j=[(k_1A-k_6)/D_0]^{1/2}x_j$. These simple steps yield the stochastic equations in the vicinity of the saddle point **S**:

$$\partial_\tau\tilde{\psi} = \hat{\nabla}^2\tilde{\psi} + \tilde{\psi} - \tilde{\psi}^2 - \tilde{\psi}\tilde{\phi} + \tilde{\xi}_1(\hat{x},\tau), \tag{11}$$

$$\partial_\tau\tilde{\phi} = \hat{\nabla}^2\tilde{\phi} + \tilde{\phi} - \tilde{\phi}^2 - \tilde{\phi}\tilde{\psi} + \tilde{\xi}_2(\hat{x},\tau), \tag{12}$$

where the rescaled noise is given by

$$\langle\tilde{\xi}_1(\hat{x},\tau)\tilde{\xi}_1(\hat{x}',\tau')\rangle = 2\left(\frac{D_0}{k_1A-k_6}\right)^{2-d/2}u^{*2}\tilde{\psi}(\hat{x},\tau) \times\delta^d(\hat{x}-\hat{x}')\delta(\tau-\tau'), \tag{13}$$

$$\langle\tilde{\xi}_2(\hat{x},\tau)\tilde{\xi}_2(\hat{x}',\tau')\rangle = 2\left(\frac{D_0}{k_1A-k_6}\right)^{2-d/2}u^{*2}\tilde{\phi}(\hat{x},\tau) \times\delta^d(\hat{x}-\hat{x}')\delta(\tau-\tau'). \tag{14}$$

In two dimensions, the noise strength is characterized by the parameter $\sigma^2=2D_0u^{*2}/(k_1A-k_6)$, with $u^*=1/\sqrt{3}\approx 0.58$, and this can be large or small depending on whether the diffusion

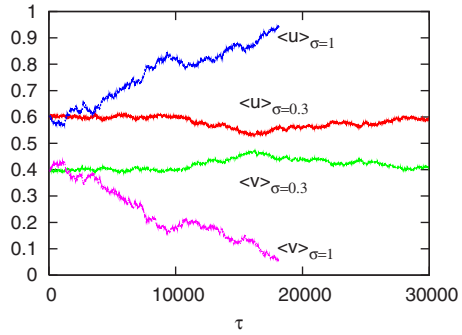

FIG. 2. (Color online) $k_4=k_5$: Time evolution of the spatially averaged enantiomer densities $\langle u\rangle=\langle\tilde{\phi}\rangle$ and of $\langle v\rangle=\langle\tilde{\psi}\rangle$ in two dimensions $d=2$ for two representative simulations of the stochastic dynamics near the saddle point **S**, Eqs. (11), (12) with noise Eqs. (13), (14). Evolution of nonracemic homogeneous initial conditions $(\tilde{\phi}(\hat{x},\hat{y},\tau=0),\tilde{\psi}(\hat{x},\hat{y},\tau=0))=(0.6,0.4)$. For weak noise $\sigma=0.3$ see the inner pair of red (dark gray) and green (light gray) curves. For stronger $\sigma=1$ noise, see the outer pair of blue (dark gray) and magenta (light gray) curves.

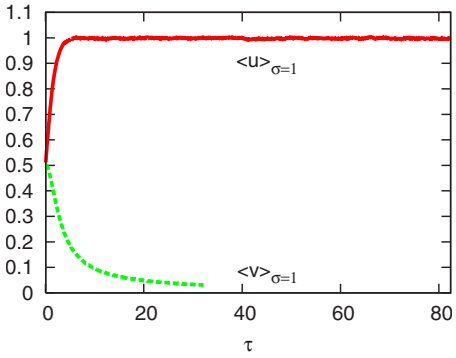

FIG. 3. (Color online) $k_4\neq k_5$: Time evolution of the spatially averaged enantiomer densities $\langle u\rangle=\langle\tilde{\phi}\rangle$ and of $\langle v\rangle=\langle\tilde{\psi}\rangle$ in two dimensions $d=2$ for a representative simulation of the stochastic dynamics near the asymmetric unidirectional fixed point **U1**, Eqs. (15), (16). Evolution of homogeneous racemic initial conditions $((\tilde{\phi}(\hat{x},\hat{y},\tau=0),\tilde{\psi}(\hat{x},\hat{y},\tau=0))=(0.5,0.5)$ for noise level $\sigma=1$. $\langle u\rangle_{\sigma=1}$ is shown in the upper solid red (dark gray) curve and $\langle v\rangle_{\sigma=1}$ is shown in the lower dashed green (light gray) curve.

rate D_0 is large or small (keeping the difference $k_1A-k_6>0$ fixed), respectively. In Fig. 2, some representative effects of the diffusion on the critical dynamics in the neighborhood of the saddle point **S** in $d=2$ are displayed for the spatially averaged enantiomers for both large ($\sigma=1$) and small ($\sigma=0.3$) internal noises and for nonracemic initial conditions. Recall that here we have set $k_4=k_5$. We solve numerically the full stochastic two-dimensional version of Eqs. (11), (12) subject to the noise given by Eqs. (13), (14), using reflecting boundary conditions and a finite difference scheme with $\Delta\tau=0.005$, $\Delta\hat{x}=\Delta\hat{y}=0.23$, and a grid of size $L\times L=154\times 154$.

For small noise levels ($\sigma=0.3$), and for nonracemic initial compositions, the initial proportion of the two chiral species is roughly maintained, modulo the fluctuations; see the inner pair of curves in Fig. 2. The evolution of $\langle u\rangle_{\sigma=0.3}$ is shown in the red (dark gray) line and $\langle v\rangle_{\sigma=0.3}$ in the green (light gray) line. However, for stronger noise ($\sigma=1$), the initial imbalance shows an almost monotonic tendency to increase, suggesting that sufficiently strong noise is capable of driving the system to a homochiral final state, in spite of the manifest mathematical chiral symmetry of the underlying evolution equations and noise terms under the substitutions $\tilde{\psi}\to\tilde{\phi}$ and $\tilde{\phi}\to\tilde{\psi}$. A mean field analysis of the solutions of Eqs. (11) and (12), which ignores both diffusion and noise, indicates that the enantiomeric excess of the concentrations of the two enantiomers is time independent [21]. Here, this is seen to be approximately true also for the spatially averaged diffusing enantiomers subject to small noise. But greater internal noise induces a striking departure from this that is not captured by the mean field approximation, as seen in Fig. 2. This is depicted in the outer pair of curves. The evolution of $\langle u\rangle_{\sigma=1}$ is shown in the blue (dark gray) line and $\langle v\rangle_{\sigma=1}$ in the magenta (light gray) line.

As we are interested here in displaying only the initial and intermediate time dependent tendencies of the two enantiomer densities in the vicinities of the various RG fixed points, we have employed standard integration of the Langevin equations, sufficient for revealing the qualitative nature of the solutions for short and intermediate computational time steps, as can be seen in Figs. 2 and 3 (below). Near an absorbing state transition, one of the densities tends to zero, and the numerical integration breaks down. This can be seen clearly in the simulation of the evolution to the absorbing state, which is shown only for the shorter time scales in these figures. This standard algorithm is of course not adequate for extracting the much more precise and delicate information such as asymptotic decays or power law exponents. For the latter, we would have had to appeal to the more sophisticated numerical schemes such as those proposed by Dickman [22], Moro [23] or by Dornic *et al.* [24].

B. Langevin equations in the vicinity of the unidirectional fixed points

The behavior of the system near one of the two stable attracting fixed points, for instance **U1**, is determined by the pair of equations

$$\partial_\tau\tilde{\psi}=\hat{\nabla}^2\tilde{\psi}+\tilde{\psi}-\tilde{\psi}^2-2\tilde{\psi}\tilde{\phi}+\tilde{\xi}_1(\hat{x},\tau), \tag{15}$$

$$\partial_\tau\tilde{\phi}=\hat{\nabla}^2\tilde{\phi}+\tilde{\phi}-\tilde{\phi}^2+\tilde{\xi}_2(\hat{x},\tau), \tag{16}$$

with the noise properties as given above in Eqs. (13), (14). Here, we use the fixed point value $(u_{12},u_{21})=(0,2u^*)$. Recall in order to arrive at this fixed point, we set $k_4\neq k_5$. This corresponds to "starting" the system off in either the basin of attraction of **U1** or that of **U2** (see the shaded quadrant in Fig. 1). Note the manifest asymmetry in the equation pair due to the presence of the unidirectional coupling term in Eq. (15), absent from Eq. (16). This fixed point is associated with homochirality, as confirmed by numerical simulation; see Fig. 3. Starting from racemic initial conditions, the plot of the spatially averaged enantiomeric densities, in Fig. 3, indicates an extremely rapid onset of absolute chiral amplification.

The evolution of $\langle u\rangle_{\sigma=1}$ is shown in the upper solid red (dark gray) curve and that of $\langle v\rangle_{\sigma=1}$ is shown in the lower dashed green (light gray) curve. The equations governing the critical dynamics at the other stable fixed point **U2** are had by simply interchanging the fields $\tilde{\psi}\leftrightarrow\tilde{\phi}$ in Eqs. (15), (16) and replacing $\tilde{\xi}_1\leftrightarrow\tilde{\xi}_2$. The behavior is quantitatively identical, but with the roles of the two enantiomers obviously reversed.

Near criticality, there is no numerical evidence for the formation of the spatially segregated chiral domains bounded by racemic fronts, in marked contrast to the results reported in [18]. The distinguishing factor of course is that the present simulations are carried out at the unidirectional critical points **U1** or **U2**, whereas in [18], the system was explored *far away* from criticality, where such chirally pure domains are expected to form [6,25]. At the RG unidirectional fixed points, the dynamical equations themselves are manifestly chirally asymmetric, and the system rapidly evolves to a final homochiral state, without passing through the intermediate stages of enantiomeric competition.

C. Stochastic dynamics away from the critical points

The distinction between the critical and noncritical behavior can be sharpened by contrasting the mathematical structure of the critical equations and noise to those that hold *away* from the fixed points. The latter are of course given by the system Eqs. (7), (8) with the fluctuations obeying Eqs. (9), (10) [26]. By means of the field rescaling $\tilde{\psi}=[(k_2+k_5)/u_0]\psi$, and with a similar relation between $\tilde{\phi}$ and ϕ, these Langevin equations can be written as (note: in what follows we take $k_4=k_5$)

$$\partial_\tau\tilde{\psi}=\hat{\nabla}^2\tilde{\psi}+\tilde{\psi}-g\tilde{\psi}^2-\tilde{\psi}\tilde{\phi}+\eta_1(\hat{\mathbf{x}},\tau), \tag{17}$$

$$\partial_\tau\tilde{\phi}=\hat{\nabla}^2\tilde{\phi}+\tilde{\phi}-g\tilde{\phi}^2-\tilde{\phi}\tilde{\psi}+\eta_2(\hat{\mathbf{x}},\tau), \tag{18}$$

where $g=k_3/(k_2+k_5)$ and the rescaled noise obeys

$$\langle\eta_1(\hat{\mathbf{x}},\tau)\eta_1(\hat{\mathbf{x}}',\tau')\rangle=2\frac{(k_2+k_5)}{D_0^{d/2}}(k_1A-k_6)^{d/2-1}\tilde{\psi}(\hat{\mathbf{x}},\tau)\times\delta^d(\hat{\mathbf{x}}-\hat{\mathbf{x}}')\delta(\tau-\tau'), \tag{19}$$

$$\langle\eta_2(\hat{\mathbf{x}},\tau)\eta_2(\hat{\mathbf{x}}',\tau')\rangle=2\frac{(k_2+k_5)}{D_0^{d/2}}(k_1A-k_6)^{d/2-1}\tilde{\phi}(\hat{\mathbf{x}},\tau)\times\delta^d(\hat{\mathbf{x}}-\hat{\mathbf{x}}')\delta(\tau-\tau'). \tag{20}$$

If the noise and the diffusion terms are ignored, then a mean field analysis of the homogeneous asymptotic solutions of the corresponding equations Eqs. (17), (18), reveals that the parameter g plays a special role [21]. Indeed, $g<1$ leads to chiral amplification of an initial enantiomeric excess, whereas $g>1$ leads to a racemic final state. The point $g=1$ was identified as a *critical* value, in the sense that a sudden qualitative change in the asymptotic behavior of the mean field solutions is observed: the ratio of the two enantiomeric concentrations in this borderline case remains constant, and depends on the initial composition. If the initial condition is racemic, the system will always remain racemic, if, however, there is a slight initial excess, this excess is forever maintained [21].

From these remarks we see that the spatially dependent and stochastic effective equations associated with each renormalization group fixed point **S**,**U1**, Eqs. (11), (12) and Eqs. (15), (16), respectively, have $g=1$. Likewise for the point **U2**. It is *as if* we had set g to its "critical" value. But it is important to emphasize that at these RG fixed points, g is no longer a freely adjustable parameter, but under renormalization is automatically driven to this special value. The RG thus provides a rational physical explanation for why $g=1$ at criticality.

V. DISCUSSION

As supported by surveys and reviews of the present status of chiral autocatalysis, mirror symmetry breaking, stochasticity, and their implications for the origin of homochirality, the Frank model and its extensions continue to serve as the paradigm for theoretical studies of this phenomenon [3–5,27]. In this paper we have studied the critical properties of the Frank model and a simple extension of it, by exploiting the mapping of this kinetic scheme to a well studied phenomenon from condensed matter and nonequilibrium statistical physics, namely, (multispecies) directed percolation processes [13]. By virtue of this exact mapping, which is established at the level of statistical field theory, the complete renormalization group (RG) analysis of the critical properties of directed percolation can be applied to study the critical features of the Frank model. The most significant result in this paper is the description of a new effect in the field of molecular chirality, namely mirror symmetry breaking induced by internal noise in extremely diluted systems with absolute enantioselective catalysis. Such a mechanism is of course vitally important for scenarios of prebiotic chemistry, where it is commonly agreed upon that sufficiently high concentrations of organic compounds could not have been reached during the chemical evolution of the early earth [28]. These final states are consequence of internal composition fluctuations and reactions limited by spatial diffusion. To reach these dilute multicritical states, the difference between the amplification and decay rates must be close to zero [13]. This contrasts to Saito and Hyuga's suggestion that, for closed systems, both *nonlinear* autocatalysis and recycling with diffusion seem to be required for chiral symmetry breaking in dilute solutions [29]. Additional insight into the dynamical consequence of each transition is provided by deriving and numerically solving the exact *effective* Langevin equations that hold in the neighborhood of each fixed point.

It has been known for some time that the chirally symmetric state of the Frank model is unstable and that (external) fluctuations can induce a transition to homochiral final states. There are evidently a number of distinct routes leading to homochirality, and the concept of criticality and the identification of the associated critical parameters should be clearly distinguished. From general bifurcation theory, we thus learn that the transition from a symmetric to a chiral

final state can be induced by varying solely the concentrations of the substrate molecules [30]. The mean field analysis of Ref. [21], on the other hand, identifies the ratio of rate constants $g=k_3/k_2$ as the pertinent critical parameter. In certain crystallization experiments, it is the *stirring rate* of the solution that has been observed to play the role of a critical parameter [31]. The present work makes use of the fact that chiral or mirror symmetry breaking is an example of an active to absorbing state phase transition, and that such transitions are generically characterized by directed percolation processes (DP) [16]. RG techniques can be applied to analyze this symmetry breaking phenomenon in extremely dilute chemical systems in a precise manner.

ACKNOWLEDGMENTS

We acknowledge useful conversations with Professor Josep M. Ribó during the course of this work. We are especially indebted to Professor Vladik Avetisov for recognizing the correct significance of our results in the context of prebiotic chemistry. We thank Dr. Carlos Briones for supplying us with the second book cited in Ref. [28]. This research was supported in part by Grant No. AYA2006-15648-C02-02 from the Ministerio de Educación y Ciencia (Spain).

APPENDIX A: CRITICAL REGIME IMPLIES EXTREME DILUTION

Simple bifurcation analysis of the purely kinetic scheme Eqs. (1)–(3)

$$\frac{dL}{dt} = (k_1A - k_6)L - k_3L^2 - (k_2 + k)LD, \tag{A1}$$

$$\frac{dD}{dt} = (k_1A - k_6)D - k_3D^2 - (k_2 + k)LD, \tag{A2}$$

reveals the chemical nature of the critical regime of the fully stochastic field theory treated in this paper [32]. Here, A, L, and D denote concentrations and we have set $k_4=k_5=k$. Introduce the enantiomeric excess $\eta=\frac{L-D}{L+D}$ and the total concentration of chiral matter $\chi=L+D$. Then the kinetic equations Eqs. (A1), (A2) can be written as follows:

$$\frac{d\eta}{dt} = \frac{k_2 + k - k_3}{2}\chi\eta(1 - \eta^2), \tag{A3}$$

$$\frac{d\chi}{dt} = (k_1A - k_6)\chi - \left[k_3 + \frac{k_2 + k - k_3}{2}(1 - \eta^2)\right]\chi^2. \tag{A4}$$

For behavior with large amount of chiral matter, $\chi \gg 0$, we must have $(k_1A-k_6) \gg 0$. This requires that the system be *far* from criticality. The bifurcation equation [1] is then $\eta(1-\eta^2)=0$ and there are three stationary solutions:

$$\left\{\eta = 0, \chi = 2\frac{k_1A - k_6}{k_2 + k + k_3}\right\}, \tag{A5}$$

unstable if $k_2-k>0$ and stable if $k_2-k<0$, and

$$\left\{\eta = \pm 1, \chi = \frac{k_1A - k_6}{k_3}\right\}, \tag{A6}$$

stable if $k_2-k>0$ and unstable if $k_2-k<0$. From this we can deduce the following salient features: First, by introducing the dimensionless time $\tau=(k_1A-k_6)t$, we see that far from criticality, the variable χ changes much more rapidly than the enantiomeric excess η. The system rapidly reaches a quasistationary state for χ ($d\chi/d\tau \approx 0$) and then the slow variable η evolves and the full system reaches its true steady state. Second, the criticality condition $(k_1A-k_6)\approx 0$ corresponds to the kinetic behavior under conditions of extreme dilution, $\chi \approx 0$, with the concentration of chiral material close to zero. In this case, the system has no well defined steady state with respect to the concentration χ, since $\eta=(L-D)/\chi$ yields an indeterminate expression near criticality. Furthermore, the equation for χ becomes as "slow" as the equation for η, and the use of classical kinetic approach based on the law of mass action becomes questionable. Thus the stochastic approach employed in this paper is not only justified, but is needed to correctly describe the critical regime of the Frank model.

APPENDIX B: REVERSIBLE REACTIONS

The backreaction of the dimerization step is eliminated if the product P is continuously being removed from the reactor. Otherwise, the reverse reaction must be taken into account. Furthermore, as pointed out by Avetisov and Goldanskii [1], reversibility in the mutual inhibition reactions will account for the limited enantioselectivity of chiral catalysts, so that the catalytic effect of each enantiomer leads to the formation of *both* L and D products. To include these effects, the following reactions would have to be added to the above scheme Eqs. (1)–(3):

$$P \xrightarrow{k_{-2}} L + D, \quad L + A \xrightarrow{k_{-4}} L + D, \quad D + A \xrightarrow{k_{-5}} L + D. \tag{B1}$$

The left-hand-most reaction corresponds to the backreaction of the dimerization, while the latter two allow for reversibility in the mutual inhibition reactions. Going through the same algebraic procedure that led us to the effective action in Sec. II, we find that the above reactions yield the following terms to be added to the effective action in Eq. (5):

$$\Delta S_{eff} = -\int d^d\mathbf{x} \int dt\{k_{-2}\theta\psi^* + k_{-2}\theta\phi^* + k_{-2}\theta^2\psi^*\phi^* + k_{-4}\phi^*\psi + k_{-5}\psi^*\phi + k_{-4}\theta\psi^*\psi\phi^* + k_{-5}\theta\phi^*\phi\psi^*\}. \tag{B2}$$

From dimensional analysis we find that $[k_{-2}\theta]=\kappa^{2+d/2}$, $[k_{-2}\theta^2]=[k_{-4}]=[k_{-5}]=\kappa^2$ are relevant perturbations in the sense of the RG for all dimensions, whereas $[k_{-4}\theta]=[k_{-5}\theta]=\kappa^{2-d/2}$. The corresponding cubic terms are therefore marginal in $d_c=4$ dimensions and are relevant for $d<4$.

From the point of view of the field-theoretic content of ΔS_{eff}, we see that the dimerization backreaction induces new relevant terms not present in the original effective action proportional to $\sim\psi^*$, $\sim\phi^*$, as well as a term of dimension

κ^2. However, this additional term proportional to $\psi^*\phi^*$ dynamically couples the two enantiomers via a cross-correlated noise, a feature not present in the absence of dimer breakup. Regarding the limited enantioselectivity reactions, these induce "masslike" terms $\sim\phi^*\psi$, $\sim\psi^*\phi$, that also serve to link the two enantiomers. In fact, these terms lead to off diagonal contributions to the response functions or propagators. The new cubic terms $\sim\psi^*\psi\phi^*$, $\sim\phi^*\phi\psi^*$ are also sources of "off-diagonal" or cross-correlated reaction noise; in graphical perturbation theory, these lead to new cubic vertices which would have to be included in a field-theoretic RG analysis, such as in [17].

[1] V. Avetisov and V. Goldanskii, Proc. Natl. Acad. Sci. U.S.A. **93**, 11435 (1996).

[2] M. Avalos, R. Babiano, P. Cintas, J. L. Jiménez, and J. C. Palacios, Tetrahedron: Asymmetry **11**, 2845 (2000).

[3] D. K. Kondepudi and K. Asakura, Acc. Chem. Res. **34**, 946 (2001).

[4] D. G. Blackmond, Proc. Natl. Acad. Sci. U.S.A. **101**, 5732 (2004).

[5] I. Weissbuch, L. Leiserowitz, and M. Lahav, Top. Curr. Chem. **259**, 123 (2005).

[6] F. C. Frank, Biochim. Biophys. Acta **11**, 459 (1953).

[7] In this paper, the symbols "*L*" (left-handed) and "*D*" (right-handed) are used to refer only to the molecule's geometrical or spatial conformation. Handedness, or chirality, is an extrinsic property. Crystal chirality can be determined from its optical activity. However, and this is the subtle point to be aware of, some left-handed molecules rotate plane polarized light in the clockwise sense, while others do so in the anticlockwise sense (and similarly for right-handed molecules). For this reason, we refrain from employing the terminology "levo" and "dextro," which refer strictly to the *intrinsic* optical properties of (chiral) molecules.

[8] P. G. H. Sandars, Origins Life Evol. Biosphere **33**, 575 (2003).

[9] A. Brandenburg, A. C. Andersen, S. Höfner, and M. Nilsson, Origins Life Evol. Biosphere **35**, 225 (2005).

[10] A. Brandenburg and T. Multamäki, Int. J. Astrobiology **3**, 209 (2004).

[11] M. Gleiser and J. Thorarinson, Origins Life Evol. Biosphere **36**, 501 (2006).

[12] M. Gleiser, Origins Life Evol. Biosphere **37**, 235 (2007).

[13] H.-K. Janssen, J. Stat. Phys. **103**, 801 (2001); Phys. Rev. Lett. **78**, 2890 (1997).

[14] M. Doi, J. Phys. A **9**, 1465 (1976); **9**, 1479 (1976).

[15] L. Peliti, J. Phys. (France) **46**, 1469 (1985).

[16] U. C. Täuber, M. Howard, and B. P. Volmayr-Lee, J. Phys. A **38**, R79 (2005).

[17] Y. Y. Goldschmidt, H. Hinrichsen, M. Howard, and U. C. Täuber, Phys. Rev. E **59**, 6381 (1999).

[18] D. Hochberg and M.-P. Zorzano, Chem. Phys. Lett. **431**, 185 (2006).

[19] M. J. Howard and U. C. Täuber, J. Phys. A **30**, 7721 (1997).

[20] In chemistry, there are no negative rate constants. As for negative diffusion, Fokker-Planck (FP) equations for certain nonlinear chemical and optical systems can have non-positive-definite diffusion coefficients. These FPs can, however, be made sense of, and a rigorous justification provided. An early paper reviewing the correct treatment of negative *D* is given in the paper by P. D. Drummond, C. W. Gardiner, and D. F. Walls, Phys. Rev. A **24**, 914 (1981).

[21] I. Gutman, D. Todorović, and M. Vučković, Chem. Phys. Lett. **216**, 447 (1993).

[22] R. Dickman, Phys. Rev. E **50**, 4404 (1994).

[23] E. Moro, Phys. Rev. E **70**, 045102(R) (2004).

[24] I. Dornic, H. Chaté, and M. A. Muñoz, Phys. Rev. Lett. **94**, 100601 (2005).

[25] P. Decker, in *Origins of Optical Activity in Nature*, edited by David C. Walker (Elsevier, New York, 1979), pp. 109–124.

[26] Apart from the noise terms, the rescaled Langevin equations for the Frank model that hold *away* from the critical regime are of course the same as those derived in Ref. [18]. The only difference comes in through the noise terms. But the mean field analysis yields the same results with the parameter *g* playing the role as indicated in Ref. [21].

[27] J. Crusats, S. Veintemillas-Verdaguer, and J. M. Ribó, Chem.-Eur. J. **12**, 7576 (2006).

[28] S. F. Mason, *Chemical Evolution* (Oxford University, New York, 1991); O. Botta and J. L. Bada, in *The Genetic Code and the Origin of Life*, edited by Ll. Ribas de Pouplana (Kluwer Academic/Plenum, New York, 2004).

[29] Y. Saito and H. Hyuga, J. Phys. Soc. Jpn. **73**, 1685 (2004).

[30] D. K. Kondepudi and G. W. Nelson, Physica A **125A**, 465 (1984).

[31] D. K. Kondepudi, K. L. Bullock, J. A. Digits, and P. D. Yarborough, J. Am. Chem. Soc. **117**, 401 (1995).

[32] We are grateful to Professor V. Avetisov for providing the calculation summarized in this Appendix and its attendant interpretation.